WATER RESOURCES RESEARCH, VOL. 46, W05511, doi:10.1029/2008WR007660, 2010

Characterizing the recharge regime of the strongly exploited aquifers of the North China Plain by environmental tracers

Christoph von Rohden,[1] Andreas Kreuzer,[1] Zongyu Chen,[2] Rolf Kipfer,[3,4] and Werner Aeschbach-Hertig[1]

Received 16 December 2008; revised 25 November 2009; accepted 16 December 2009; published 11 May 2010.

[1] We employed environmental tracers (^{3}H-^{3}He, noble gases, stable isotopes ^{18}O and ^{2}H) to study groundwater recharge and residence times in the strongly exploited North China Plain aquifer system in the area of Shijiazhuang, the capital of the Hebei province. Groundwater in the unconfined parts of the piedmont plain contains tritium down to depths of about 100 m and exhibits ^{3}H-^{3}He ages of less than 40 years. ^{3}H-^{3}He ages correlate well with sampling depth but less so with distance along a transect from the mountains in the west through the recharge area in the piedmont plain, indicating a minor role of lateral inflow compared to spatially distributed recharge. The increase of groundwater age with increasing thickness of the saturated zone combined with the steady groundwater table descent over the last decades implies an effective recharge rate of around 0.3 m/yr, mostly due to infiltration of precipitation and irrigation water. Despite the recycling of irrigation water, a water balance deficit remains, causing depletion of the aquifers. Anthropogenic modifications of the natural recharge regime appear to be reflected by a trend of increasing stable isotope ratios in groundwater of the last decades.

Citation: von Rohden, C., A. Kreuzer, Z. Chen, R. Kipfer, and W. Aeschbach-Hertig (2010), Characterizing the recharge regime of the strongly exploited aquifers of the North China Plain by environmental tracers, *Water Resour. Res.*, *46*, W05511, doi:10.1029/2008WR007660.

1. Introduction

[2] The North China Plain (NCP) is the largest alluvial plain and one of the most densely populated regions in eastern Asia. Population, economic activity, and agricultural production of the area have grown strongly over the last decades, resulting in increased water demand [*Foster et al.*, 2004]. Except for a few larger streams that have water seasonally, groundwater is the main source for industrial, domestic, and agricultural water supply. In particular, the increase of crop yields in this semiarid area was made possible only by intensive use of groundwater for irrigation since the 1960s [*Kendy et al.*, 2004]. The region produces important fractions of China's supply of wheat and corn. However, the combination of falling groundwater levels, decreasing surface water inflow, and increasing water demand threatens the sustainability of water resources and agriculture [*Yang et al.*, 2002; *Foster et al.*, 2004].

[3] Increasing exploitation of the NCP aquifer system has led to a regional decline of groundwater levels, the local formation of depression cones of the potentiometric surface in the area of large cities, and a degradation of water quality since the 1970s [*Chen et al.*, 2005; *Foster et al.*, 2004; *Lu et al.*, 2008]. In order to guide the management of the groundwater resource, several studies have addressed the water balance and recharge mechanisms in the NCP, often using geochemical and isotopic indicators [*Chen et al.*, 2003b, 2004, 2005; *Kendy et al.*, 2003, 2004]. While the paleowaters of the deep confined aquifer have been quantitatively radiocarbon-dated [*Chen et al.*, 2003a], only qualitative information on groundwater residence times derived from tritium (^{3}H) is available in the recharge zone [*Chen et al.*, 2003b, 2005; *Lu et al.*, 2008]. Consequently, considerable uncertainty remains with regard to recharge mechanisms and rates as well as vertical and horizontal flow velocities [*Lu et al.*, 2008].

[4] Several environmental tracer methods are available for the dating of young groundwater and have proven to be useful tools to assess recharge rates and groundwater flow velocities [e.g., *Cook and Solomon*, 1997; *Solomon et al.*, 1995; *Kipfer et al.*, 2002]. In this study, we employ the ^{3}H-^{3}He method [*Tolstikhin and Kamenskiy*, 1969]. Additional information that helps to constrain recharge conditions and corrections for the age dating is obtained by the use of atmospheric noble gases [*Kipfer et al.*, 2002] and stable isotopes ^{18}O and ^{2}H.

[5] Based on measurements of these environmental tracers we investigate the essential characteristics of the young groundwater with ages in the range of 0–40 years with respect to recharge mechanisms and rates. Data are interpreted in the context of the anthropogenic impact, that is, groundwater pumping and agricultural irrigation, which cause changes of the groundwater flow regime by local

[1] Institute of Environmental Physics, University of Heidelberg, Heidelberg, Germany.
[2] Institute of Hydrogeology and Environmental Geology, Chinese Academy of Geological Sciences, Zhengding, China.
[3] Department of Water Resources and Drinking Water, Swiss Federal Institute of Aquatic Science and Technology, Duebendorf, Switzerland.
[4] Institute of Isotope Geochemistry and Mineral Resources, ETH Zurich, Zurich, Switzerland.

0043-1397/10/2008WR007660

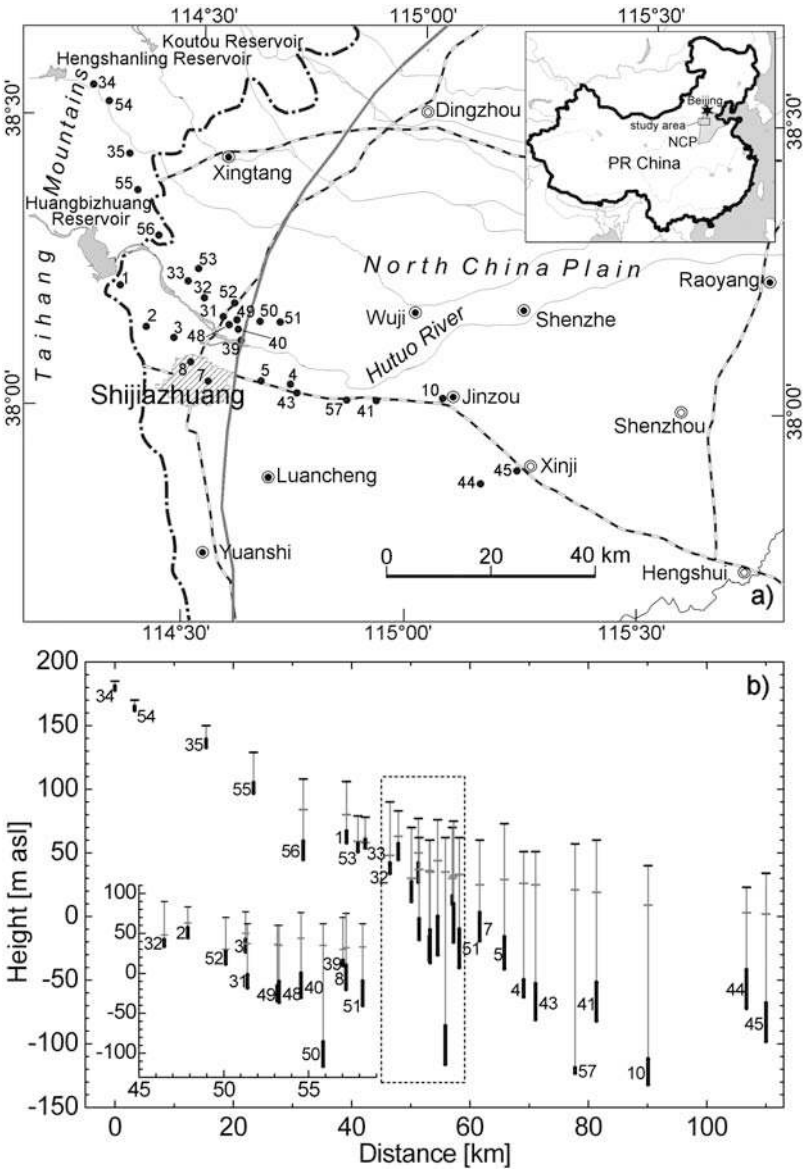

Figure 1. (a) Map of the investigation area, ~250 km south of Beijing, China. The numbers refer to the sampled wells. The dash-dotted line indicates the western border of the North China Plain (NCP); the gray line denotes the transition from unconfined to confined aquifers. The recharge area for the confined aquifers of the NCP lies between the two lines in the piedmont region. (b) Cross section showing the surface elevation, depth of the water table, and screen position for all wells. The inset shows an enlarged subset from the central part, bordered by the dashed-line box.

disturbance and regional groundwater table decline. The consequence is a substantial modification of the natural recharge characteristics.

2. Study Area

[6] Our study area lies in the northern part of the North China Plain, also referred to as the Hebei or Haihe Plain, where major cities such as Beijing, Tianjin, and Shijiazhuang are located. This part of the NCP extends from the Taihang Mountains in the west at ~150 m above sea level (asl) to the Bohai Sea in the east and from the Yanshan Mountains in the north toward the Yellow River in the south, covering an area of about 150,000 km^2. It is densely populated, with more than 100 million inhabitants, and constitutes a center of the economy and agriculture of China. The climate is continental semiarid with a mean annual temperature of about 13°C and annual precipitation between 500 and 600 mm [*Chen et al.*, 2005]. The 1955–1999 mean at Shijiazhuang was 538 mm according to monitoring data from the Beijing Climate Center (http://www.bcc.cma.gov.cn). About 70% of the total precipitation falls in the monsoon season from June to August.

[7] This study focuses on the western part of the NCP, the so-called piedmont plain, around the city of Shijiazhuang. The Quaternary sedimentary strata in the piedmont plain consist of a series of alluvial fans. Shijiazhuang is located on the large fan of the Hutuo River. The aquifer in the proximal fan is a single unconfined gravelly layer with a thickness up to about 200 m, while downstream of the midfan, a multilayer aquifer system with confined aquifers exists. There the

Table 1. Well Data and Field Measurements[a]

	Sampling Date, YMD	Long. (°)	Lat. (°)	Alt. (m asl)	Distance From Well 34 (km)	Well Depth (m)	Depth to Water (m)	Screen Interval (m)	Temp. (°C)	κ_{25}(μS/cm)	O_2(mg/L)	pH
1	20040311	114.3168	38.2086	106	39	50	26	39–48	15.6	760	n.m.	7.7
2	20040311	114.3765	38.1383	83	48	40	23	26–38	15.6	1071	n.m.	7.5
3	20040311	114.4365	38.1203	77	51	52	27	35–50	15.7	916	n.m.	7.6
4	20040312	114.6931	38.0450	51	69	120	25	101–114	14.7	525	n.m.	8.0
5	20040312	114.6263	38.0462	73	66	120	42	89–114	15.0	800	n.m.	7.7
7	20040312	114.5151	38.0441	60	62	89	40	57–79	16.7	1232	n.m.	7.2
8	20040312	114.4736	38.0742	75	57	100	46	65–95	15.9	1044	n.m.	7.6
10	20040313	115.0240	38.0258	40	90	180	31	152–172[b]	16.5	510	n.m.	7.6
31	20050406	114.5431	38.1581	62	51	80	25	64–80	14.8	757	n.m.	7.4
32	20050403	114.5037	38.1913	90	46	60	42	48–56	14.5	935	n.m.	7.4
33	20050403	114.4669	38.2185	78	42	28	20	17.5–24	14.5	930	n.m.	7.4
34	20050404	114.2425	38.5561	185	0	9	3[b]	4–7	11.4	655	5.1	7.3
35	20050404	114.3315	38.4362	150	15	19	10	11–17	14.9	707	9.6	7.3
39	20050406	114.5841	38.1183	70	57	61	39	54–60	17.4	773	3.5	7.4
40	20050406	114.5741	38.1397	76	55	110	32	76–106	14.9	768	2.3	7.4
41	20050408	114.8797	38.0211	60	81	150	41	112–142[b]	15.6	495	0.3	7.7
43	20050408	114.7095	38.0317	51	71	150	26	104–132	14.8	629	0.8	7.6
44	20050409	115.1124	37.8813	23	107	100	20	65–95	15.6	992	3.8	7.6
45	20050409	115.1909	37.9039	34	110	140	32	102–132[b]	15.4	1106	0.3	7.5
48	20050411	114.5589	38.1460	60	53	100	35	70.6–96	14.8	735	3.3	7.5
49	20050411	114.5722	38.1536	60	53	98	34	76–94	15.3	779	2.6	7.4
50	20050416	114.6236	38.1519	62	56	186	27	148–178[b]	13.5	541	2.3	7.5
51	20050411	114.6669	38.1518	62	58	110	29	72–102[b]	16.5	367	4.7	7.6
52	20050412	114.5667	38.1835	70	50	60	40	43–58	15.0	794	9.5	7.5
53	20050412	114.4872	38.2402	79	41	30	20	22–28	15.5	832	9.3	7.3
54	20050414	114.2666	38.5325	170	3	12	2[b]	5–8	13.3	570	0.9	7.4
55	20050414	114.3588	38.3660	129	23	40	8[b]	24–32	15.2	653	9.6	7.4
56	20050414	114.3992	38.2974	108	32	75	24	49–63	14.1	729	10.3	7.4
57	20050416	114.8174	38.0213	57	78	180	35	176–180	16.0	496	0.8	7.5

[a]YMD is year, month, day; read 20040211 as 11 Mar 2004. Abbreviations are as follows: asl, above sea level; n.m., not measured.
[b]Estimated.

upper unconfined aquifer is about 60 m thick and is formed by coarse-grained sand. Below about 100 m depth a series of three confined aquifers follows. The sediments of all layers become increasingly fine in flow direction, typically changing from sandy gravel in the piedmont plain to medium to fine sands in the central plain. The underlying bedrock is formed by Archean gneiss and Proterozoic carbonates [*Chen et al.*, 2005].

[8] The unconfined western part of the piedmont plain constitutes the main recharge area of the NCP groundwater system [*Foster et al.*, 2004]. Further east, only the upper unconfined aquifer receives direct recharge, whereas the confined aquifers are fed by lateral inflow from the piedmont [*Chen et al.*, 2005]. The recharge in the piedmont region is made up of several contributions: precipitation, irrigation return flow, infiltration from rivers and canals, and lateral inflow from the Taihang Mountains [*Yang et al.*, 2002]. *Fei* [1988] attributed 70%– 80% of the recharge to precipitation and the rest mainly to surface water seepage. *Kendy et al.* [2004] showed that areal recharge in the form of irrigation return flow is substantial. Recharge by surface water must have diminished after the construction of reservoirs in the mountains. Since 1980, water flow was observed in the riverbeds only in the flooding seasons of 1988 and 1996 [*Yang et al.*, 2002]. Different opinions exist on the importance of lateral inflow from the mountains. *Fei* [1988] estimated it to account for only 2% of the total recharge, whereas *Chen et al.* [2003b] postulated it to be the major recharge component.

[9] A total of 52 wells were sampled in two campaigns in March 2004 and April 2005 across the entire NCP. This study is based on a subset of 29 wells along a ~120 km transect starting at the eastern rim of the Taihang Mountains, crossing the piedmont plain in southeastern direction, and extending into the central part of the NCP (Figure 1a). Except for four samples from the mountain area to the west of the NCP (wells 34, 35, 54, and 55), noble gas and stable isotope data have been reported before in a paleoclimate study [*Kreuzer et al.*, 2009]. That study included additional wells further downstream in the central and coastal plain containing ^{14}C-dated groundwater of Holocene and Pleistocene age. Selection criterion for the wells used here was a comparatively young, that is, not ^{14}C-datable, groundwater age. This criterion also coincides with well depths less than 200 m. The present study focuses on the results obtained from the ^{3}H-^{3}He dating method and their implications with regard to groundwater recharge in the piedmont area.

[10] Figure 1b provides a schematic cross section through the study area along the sampled transect, showing the local vertical positions of the ground surface, the water table, and the well screen for each well. The distance scale is given by the linear distance of each well from the westernmost well 34. A major feature of this cross section is that well depths increase rather systematically with distance because the thickness of the sedimentary layers grows and the depth of layers bearing usable groundwater increases in eastward direction. Since most wells have rather short screens, the vertical age structure within the aquifer system can be resolved reasonably well.

Table 2. ^{3}H Concentrations, He Isotopes, and ^{3}H-^{3}He Ages[a]

	He ($\times10^{-8}$) (cm^3 STP/g)	±He ($\times10^{-8}$) (cm^3 STP/g)	^{3}He/ ^{4}He ($\times10^{-6}$)	±^{3}He/ ^{4}He ($\times10^{-6}$)	He_{rad} ($\times10^{-9}$) (cm^3 STP/g)	±He_{rad} ($\times10^{-9}$) (cm^3 STP/g)	^{3}H (TU)	±^{3}H (TU)	^{3}H-^{3}He age (yr)	±^{3}H-^{3}He age (yr)	ΔNe (%)	Group
1	7.85	0.06	1.62	0.010	23.9	1.3	15.4	1.4	15.2	1.0	16.8	R
2	14.75	0.13	0.69	0.003	92.5	1.7	17.6	1.4	7.2	0.7	19.2	R
3	6.65	0.06	1.25	0.008	16.9	0.9	17.8	1.4	5.2	0.5	8.4	R
4	5.07	0.04	1.47	0.009	3.4	1.3	0.0	1.0	n.e.	n.e.	3.2	S
5	6.31	0.05	1.94	0.008	1.2	1.3	11.0	1.2	15.5	1.2	29.9	D
7	8.12	0.07	1.24	0.009	24.9	1.1	13.8	1.5	9.0	0.9	22.0	D
8	6.49	0.06	1.36	0.008	14.0	0.9	17.9	1.5	6.2	0.6	11.8	D
10	5.55	0.05	1.29	0.008	9.0	1.3	0.0	1.1	n.e.	n.e.	1.9	S
31	7.46	0.06	3.09	0.013	3.8	2.0	19.5	1.5	23.7	1.1	52.9	R
32	7.15	0.04	2.23	0.013	2.3	0.9	19.2	1.6	15.3	0.9	48.8	R
33	6.86	0.06	2.02	0.014	3.9	1.8	17.0	1.4	14.0	1.0	39.9	R
34	11.10	0.05	0.87	0.007	58.1	0.8	6.9	1.4	14.6	2.2	18.0	M
35	5.47	0.02	1.43	0.013	0.4	0.6	17.3	1.5	1.6	0.4	21.5	R
39	7.49	0.04	2.87	0.015	2.5	0.9	9.3	1.4	32.0	2.2	58.1	R
40	6.40	0.04	4.45	0.021	3.5	0.8	12.6	1.5	35.9	1.9	30.1	R
41	5.99	0.03	1.24	0.011	10.8	0.7	0.0	1.3	n.e.	n.e.	7.0	S
43	5.27	0.03	1.70	0.011	3.1	0.7	2.9	1.3	25.3	6.3	7.5	S
44	6.22	0.03	2.31	0.013	10.0	0.6	15.7	1.2	18.7	0.9	13.7	L
45	5.74	0.03	2.70	0.017	2.3	0.8	4.0	1.2	40.6	5.4	20.4	S
48	6.99	0.04	4.00	0.015	3.6	0.9	19.2	1.3	28.5	1.0	41.6	R
49	7.56	0.04	2.73	0.015	19.5	0.8	10.5	1.4	31.7	2.0	21.7	R
50	7.32	0.04	1.33	0.010	18.3	0.8	1.3	1.2	n.e.	n.e.	19.5	S
51	13.71	0.06	n.m.	n.m.	47.0	1.7	0.9	1.4	n.e.	n.e.	n.e.	S
52	5.55	0.03	2.18	0.013	1.3	0.6	6.8	1.2	23.9	2.3	18.8	R
53	6.88	0.03	2.34	0.011	9.5	0.7	24.8	1.3	14.8	0.5	29.7	R
54	12.14	0.10	1.18	0.008	65.8	1.9	19.8	1.6	14.7	0.9	22.2	M
55	5.60	0.03	1.49	0.013	1.1	0.7	9.4	1.5	5.5	1.0	21.8	R
56	7.30	0.03	3.39	0.018	−1.0	0.9	18.9	1.4	25.2	1.0	60.1	R
57	5.49	0.05	1.34	0.012	7.9	1.3	0.6	1.3	n.e.	n.e.	2.9	S

[a]Uncertainties are given as 1σ errors. For study group, abbreviations are as follows: D, depression = modern samples from area of Shijiazhuang depression cone; L, local lens = shallow well in the central plain; M, mountains = modern samples from mountain region; R, regular = "regular" modern sample; S, submodern = submodern mixed or old samples (low or no ^{3}H). Additional abbreviations are as follows: n.e., not evaluated; n.m., not measured; TU, tritium units.

[11] Although the sampled transect was chosen to follow the general flow direction, not all wells represent a continuous evolution. Of the four samples from the foothills of the Taihang Mountains, at least the two westernmost and shallowest wells (34, 54) represent local shallow groundwater flow systems in river valleys that are not directly connected with the aquifers in the NCP. The samples from the 2004 campaign (wells 1–10) partly lie on a somewhat more southerly transect which passes through the depression cone of the city of Shijiazhuang. Therefore, some of these wells (especially 5, 7, and 8) may be influenced by mixing induced by the heavy pumping in the area and other anthropogenic effects.

[12] The boundary of the confined aquifers lies just east of Shijiazhuang, near well 39 (Figure 1a). Most wells to the west represent the phreatic alluvial fan flow system, where recharge takes place. Turnover times in this part of the aquifer system have been estimated to be less than 200 years [*Zhang et al.*, 1987]. Most wells to the east tap the regional flow system made up by the confined aquifers. Well depths range from 28 to 110 m in the unconfined part of the NCP aquifer system (Figure 1b and Table 1). In the confined part, wells are deeper than 110 m. Well 44 may represent an exception, which, at a depth of only 80 m, may tap a local lens of shallow, fresh groundwater [*Foster et al.*, 2004; *Zhang et al.*, 1987]. This depth classification reflects the two-layered structure of the groundwater noted by several authors [*Chen et al.*, 2004; *Fei*, 1988; *Lu et al.*, 2008], with a boundary at about 80–100 m depth separating geochemically and isotopically distinct waters.

[13] As a consequence of groundwater pumping over the last several decades, the depth of the groundwater table in the unconfined area is typically about 30 m, albeit with a certain variability. The depth to water ranges from less than 10 m in the mountain area to more than 40 m in the depression cone around Shijiazhuang. In the remaining part of the unconfined area studied here, it ranges between about 20 and 40 m.

3. Methods

[14] Samples were taken from municipal or agricultural wells that are in routine use and equipped with submersible pumps. Since only incomplete documentation of the wells was available, information on well characteristics such as screened interval and depth to water had to be gathered from various sources, including drilling companies and maps of the hydraulic head distribution prepared by the Institute of Hydrogeology and Environmental Geology (IHEG) at Zhengding. The data are summarized in Table 1. The wells are screened close to their lower ends with screen lengths between 3 and 30 m (15 m on average). For five wells no screen information was available. Assuming that all wells were constructed similarly, we assigned screen intervals of 30 m length to these wells. Sample depths were assigned to the center of the screened sections.

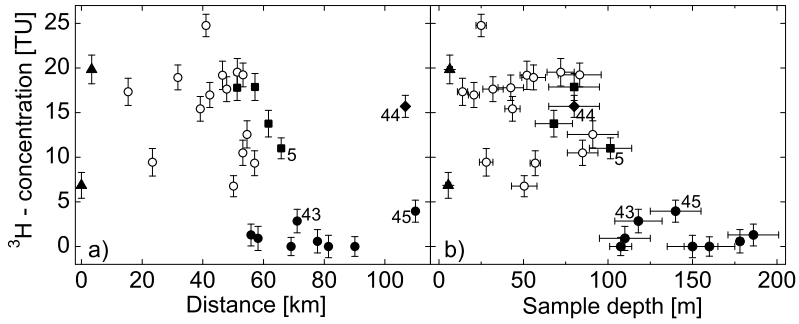

Figure 2. Measured tritium concentrations versus distance along (a) the transect and (b) well depth. Modern (^{3}H-bearing) samples from the unconfined part of the piedmont plain ("regular" samples) are indicated by open circles. Solid symbols refer to the following distinguished groups: samples from river valleys within the Taihang Mountains (triangles), samples within a depression cone due to strong pumping in the urban area of Shijiazhuang (squares), well 44 tapping a local shallow freshwater lens in the central plain (diamond), and submodern, that is, ^{3}H-free or mixed (^{3}H < 5 tritium units (TU)) samples from the confined part of the NCP (solid circles). The classification and symbol formatting is kept consistent for Figures 2–7 and 9.

[15] Wells were sufficiently flushed before sampling to purge the water in the borehole. At large-diameter (10–15 cm) agricultural wells a flexible hose was fitted over the pipe to collect all the water from the well pipe. It was connected to a full-metal flow divider with three outlets, each controlled by a valve, to split the water flow and regulate pressure. Two outlets were used to divert excess water, and on the third a tight combination of tubing was used to reduce the diameter to 10 mm for connection with the copper tube samplers used for noble gases. The entire setup was flushed until no gas bubbles were visible.

[16] Temperature, electrical conductivity, pH, and dissolved oxygen (only in 2005) were measured in the field (Table 1). Major ions were analyzed at the IHEG. Water samples for measurements of stable isotopes ^{18}O and ^{2}H were taken in 50 ml glass bottles and analyzed at the Institute of Environmental Physics (IUP) in Heidelberg, Germany, on a Finnigan MAT 252 mass spectrometer. Samples for tritium were taken in 100 mL glass bottles and analyzed at IUP by low-level counting after conversion into H_2 gas. The precision for long counting times is about 1 tritium unit (TU), and the detection limit on a 2σ level is therefore ~2 TU. Helium isotopes and other noble gases were analyzed at the Institute of Isotope Geochemistry and Mineral Resources of ETH Zurich, Switzerland.

[17] The ^{3}H-^{3}He method assumes the accumulation of ^{3}He from ^{3}H decay under closed conditions. It requires the separation of the different contributions to the total measured ^{3}He concentration in groundwater, including in particular the atmospheric equilibrium and excess air components [*Schlosser et al.*, 1988; *Kipfer et al.*, 2002]. The atmospheric noble gas data (Ne, Ar, Kr, Xe) and the so-called "closed-system equilibration" (CE) model [*Aeschbach-Hertig et al.*, 2000, 2008] were used to calculate the atmospheric He components. By an inverse modeling procedure [*Aeschbach-Hertig et al.*, 1999] the model parameter set was determined that provides the best fit of the model to the observed atmospheric noble gas concentrations. The resulting best values for the recharge temperatures and the excess air parameters of the CE model were reported by *Kreuzer et al.* [2009].

[18] For the ^{3}H-^{3}He dating, the atmospheric components of the He isotopes were calculated using the model parameters derived from fitting the atmospheric noble gas data. The difference between the measured total and modeled atmospheric ^{3}He and ^{4}He concentrations then yields the nonatmospheric He components, which were further separated into radiogenic and tritiogenic contributions. For the radiogenic ^{3}He/^{4}He ratio, a value of 6.1×10^{-8} determined from ^{3}H-free wells in the study region [*Kreuzer et al.*, 2009] was used. The tritiogenic ^{3}He$_{tri}$ was finally used together with ^{3}H to calculate apparent ^{3}H-^{3}He ages according to the usual age equation. The correction for radiogenic He generally has only a minor effect on the calculated ages, with the exception of a few wells with relatively high contents of radiogenic He (wells 2, 34, and 54; see Table 2).

4. Results

[19] Tritium concentrations are given in Table 2 and plotted along the sampling transect (linear distance from the westernmost well in the Taihang Mountains) and against sample depth, respectively, in Figure 2. Compared to previous studies in which tritium was used to characterize the age structure qualitatively [*Chen et al.*, 2003b, 2004, 2005; *Lu et al.*, 2008], our tritium data give a rather definite picture. Modern groundwater with about 7–20 TU gives way to water with very low tritium, which must have recharged before the onset of thermonuclear bomb testing in 1954, at a distance of approximately 60 km and a depth of about 100 m. This transition is rather clear-cut and almost exactly coincides with the transition from unconfined to confined conditions (at about 114.6°E, gray line in Figure 1a). Exceptions are the tritium-bearing wells 5 and 44. Well 5 with a sampling depth of 102 m lies in the transition zone. Well 44 is located far to the east, but with a screen depth of only 80 m it probably draws at least part of its water from the overlying unconfined aquifer.

[20] This study only includes wells from the upstream part of the confined aquifers where no significant ^{14}C ages were found [*Kreuzer et al.*, 2009]. Following a classification suggested by [*Clark and Fritz*, 1997], we divide these

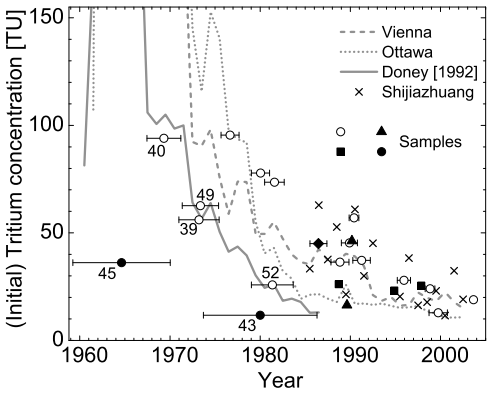

Figure 3. Initial tritium ($^3H + {}^3He$) versus recharge year obtained from the apparent ^3H-^3He ages, along with records of yearly mean tritium in precipitation at Shijiazhuang (crosses), Vienna (dashed line), and Ottawa (dotted line). The solid line indicates a model reconstruction of the local tritium input according to *Doney et al.* [1992]. Groups and symbols as in Figure 2.

"young" samples into a modern group ($^3H > 5$ TU), a submodern group (no significant ^3H), and a category indicated by a mixture of tritium-free prebomb groundwater and young tritium-containing water (low but measurable ^3H, wells 43 and 45). Within the modern group, reasonably precise ages can be determined by the ^3H-^3He dating technique (Table 2). The apparent ^3H-^3He ages of the mixed samples have large uncertainties and are not deemed reliable since they do not reflect the unknown fraction of tritium-free prebomb water in these wells. Since neither the mixed nor the submodern samples can effectively be dated, they are in the following subsumed as submodern, meaning that the bulk of their water has an age somewhere between the upper limit of the ^3He-^3He method (~50 years) and the lower limit of ^{14}C dating of groundwater (~1000 years). In Figure 2, as well as in Figures 3–7 and 9, the submodern samples are distinguished from the modern samples and represented as solid circles.

[21] Using the geographic and hydrogeologic setting, we introduce additional subgroups among the modern wells. The following four groups are differentiated in Figures 2–7 and 9: The "regular" modern samples from the unconfined part of the piedmont plain (open circles), the samples from the Taihang Mountains (wells 34 and 54, solid triangles), the samples from the depression around Shijiazhuang (wells 5, 7, and 8, solid squares), and the far downstream but shallow well 44 representing a local flow system (solid diamond).

[22] Mixing with tritium-free water is indicated if the initial tritium ($^3H + {}^3He_{tri}$) of a sample falls below the tritium concentration expected based on its apparent age and the tritium input history in precipitation (e.g., *Aeschbach-Hertig et al.* [1998]). Despite the scarcity of historic tritium data in our case, a comparison of the initial tritium concentrations reconstructed from the samples and the tritium input in precipitation over time is attempted in Figure 3. Available yearly mean tritium data in precipitation for Shijiazhuang between 1985 and 2002 are plotted as crosses. Tritium input in the study region was quite high over this period, with a weighted mean above 30 TU and only 5% of the monthly values below 10 TU. Initial tritium values of all groundwater samples that according to their ^3H-^3He ages infiltrated during this period fall in the same range. This agreement confirms the reliability of the dating and rules out significant admixing of old groundwater to these modern samples.

[23] To account for the period before 1985, the long-ranging tritium input curves for Vienna and Ottawa are also shown in Figure 3 along with an estimated local input curve for the period 1960–1986 derived from the model function presented by *Doney et al.* [1992]. For the period after 1985, the Vienna and Ottawa curves fall in the lower range of the actual data. The model estimate is considerably lower than the Vienna and Ottawa curves throughout and also below the Shijiazhuang data during the short overlap. Therefore, it appears that the Vienna and Ottawa data provide a more plausible estimate of the local tritium concentrations in precipitation before 1985. Despite the uncertainty of the input curve before 1985, the reconstructed initial tritium of wells 43 and 45 falls clearly below any reasonable estimate, confirming the classification of these samples with tritium concentrations below 5 TU as mixtures with old, tritium-free water. The oldest of the samples classified as modern (wells 39, 40, and 49) and well 52 also fall below the Vienna and Ottawa curves but are in agreement with the input estimate according to *Doney et al.* [1992]. It can therefore not clearly be decided whether or not these wells contain a fraction of prebomb water. The overall conclusion we derive from Figure 3 is that the modern samples with ages up to about 30 years show no indication of mixing with prebomb water.

[24] The apparent ^3H-^3He ages of the modern samples, but not the mixed samples 43 and 45, are therefore con-

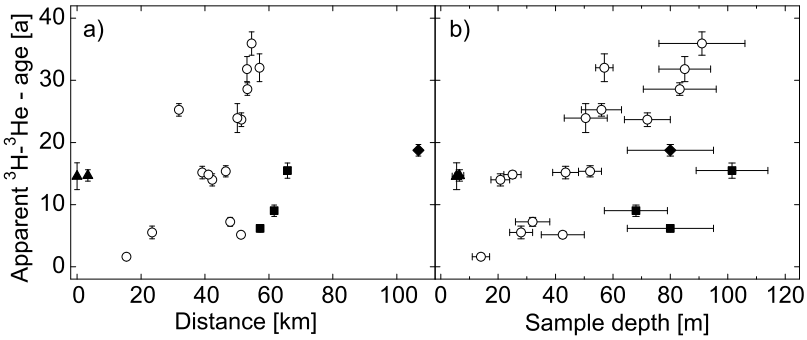

Figure 4. Apparent ^3H-^3He age versus distance (a) along the sampled flow path and (b) versus well depth. Groups and symbols as in Figure 2.

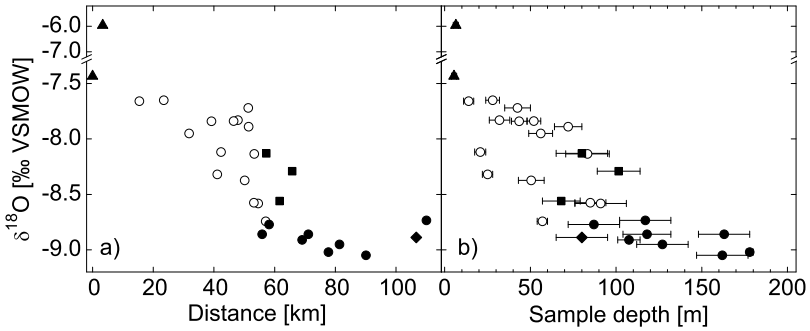

Figure 5. $\delta^{18}O$ values versus (a) distance and (b) well depth. Groups and symbols as in Figure 2. Note the scale break in the $\delta^{18}O$ axis to accommodate the exceptionally high value of one mountain well (well 54). VSMOW, Vienna standard mean ocean water.

sidered as reasonably reliable estimates of the mean residence time of the sampled groundwater in the saturated zone. These ages, ranging from 1 to 36 years (Table 2), are shown in Figure 4 versus distance along the transect as well as versus sampling depth.

[25] An increase of age with distance may be expected if lateral inflow from the mountain front is the main groundwater source, whereas an increase of age only with depth should result from spatially uniform recharge in vertical direction into a homogeneous unconfined aquifer [*Vogel*, 1967]. However, neither relationship is clearly evident from the overall figures. To clarify the picture, the different sample groups defined above should be considered separately.

[26] The two samples from the mountain region (Figure 4, solid triangles) are expected to be very young based on their upstream location and shallow depths. Surprisingly, this is not the case. This finding supports the view that these wells belong to a local flow system that is not necessarily connected to the rest of the sampled transect.

[27] The samples from the extended depression of the potentiometric surface around Shijiazhuang (Figure 4, solid squares) are surprisingly young in view of their downstream location and large depths. We assume that the local groundwater regime is disturbed by enhanced mixing and accelerated vertical and lateral flow, leading to the comparatively young apparent ages of these samples. The sample from the distant (107 km) but rather shallow (80 m) well 44 is surprisingly young for its large distance but only slightly younger than samples from similar depth in the piedmont area. Its apparent ^3H-^3He age of 19 years is inconsistent with the location downstream of several tritium-free wells. This sample obviously cannot be explained by horizontal flow but possibly indicates local recharge to the upper aquifers at this location in the central plain.

[28] The "regular" piedmont samples (Figure 4, open circles), ranging in distance between 15 and 57 km and at screen depths between 14 and 91 m, cover the entire age range and show increasing trends with distance and depth. However, the relationship of age with distance (Figure 4a) appears more irregular especially in the region between 32 and 47 km, where even a negative trend may be supposed. Comparison with Figure 4b and the cross section of Figure 1b shows that the irregularities in this region may largely be due to variations in well depth. This becomes clearer if the main northern flowline downstream of well 56 and the southern flowline southeast of well 1 are considered separately. On both lines, relatively high ages in the first wells are followed by lower ages, before an increase with distance starts. This trend is reflected by well depths, which decrease after wells 56 and 1 on both flowlines before they increase again. As already observed for well 44, apparently irregular

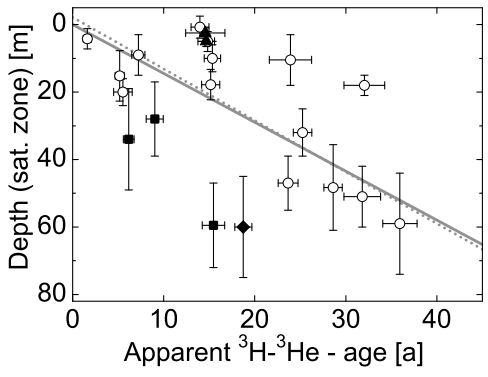

Figure 6. ^3H-^3He tracer ages versus "saturated" depth. Groups and symbols as in Figure 2. The gray line is a linear regression to the "regular" samples (open circles) and forced through the origin. The slope of the fit represents an overall estimate of the effective recharge.

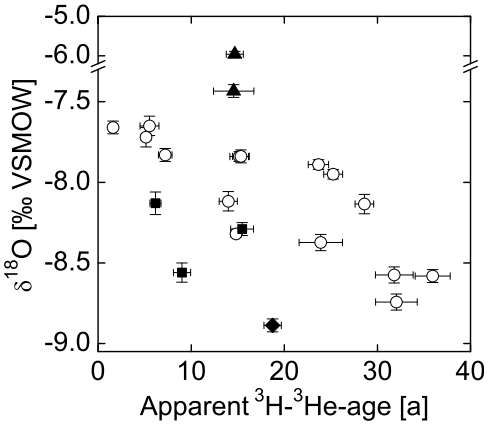

Figure 7. $\delta^{18}O$ values for modern samples versus apparent ^3H-^3He ages. Groups and symbols as in Figure 2. Note the scale break in the $\delta^{18}O$ axis to accommodate the exceptionally high value of one mountain well (well 54).

Table 3. Stable Isotopes and Chemical Data[a]

	δ^2H	$\pm\delta^2$H	δ^{18}O	$\pm\delta^{18}$O	K^+	Na^+	Ca^{2+}	Mg^{2+}	HCO_3^-	Cl^-	SO_4^{2-}
1	−58.7	0.1	−7.84	0.03	2.1	30	80	25	207	34	150
2	−58.5	0.1	−7.83	0.04	1.4	27	104	30	260	52	131
3	−58.0	0.1	−7.72	0.06	2.5	37	119	41	204	62	218
4	−65.9	0.1	−8.91	0.04	1.7	21	69	24	220	37	84
5	−62.3	0.1	−8.29	0.04	1.7	29	90	24	233	44	103
7	−62.4	0.1	−8.56	0.06	1.3	46	154	38	369	110	122
8	−60.4	0.1	−8.13	0.07	1.4	32	82	30	195	46	147
10	−66.6	0.1	−9.05	0.04	2.1	28	46	19	243	16	37
31	−58.0	0.1	−7.89	0.03	2.5	37	119	41	204	62	218
32	−57.8	0.1	−7.84	0.04	7.9	7	43	7	146	9	12
33	−58.9	0.1	−8.12	0.06	2.0	16	91	15	249	31	70
34	−54.5	0.1	−7.43	0.04	n.m.	n.m.	n.m.	n.m.	n.m.	n.m.	n.m.
35	−56.0	0.1	−7.66	0.04	n.m.	n.m.	n.m.	n.m.	n.m.	n.m.	n.m.
39	−64.5	0.2	−8.74	0.05	1.8	22	95	34	293	21	108
40	−62.9	0.1	−8.58	0.04	n.m.	n.m.	n.m.	n.m.	n.m.	n.m.	n.m.
41	−65.4	0.2	−8.95	0.04	2.3	19	67	23	242	36	54
43	−65.0	0.2	−8.86	0.04	1.8	22	95	34	293	21	108
44	−64.9	0.2	−8.89	0.04	n.m.	n.m.	n.m.	n.m.	n.m.	n.m.	n.m.
45	−64.0	0.2	−8.73	0.06	n.m.	n.m.	n.m.	n.m.	n.m.	n.m.	n.m.
48	−60.5	0.2	−8.13	0.06	n.m.	n.m.	n.m.	n.m.	n.m.	n.m.	n.m.
49	−63.1	0.2	−8.57	0.05	n.m.	n.m.	n.m.	n.m.	n.m.	n.m.	n.m.
50	−64.3	0.2	−8.86	0.06	1.7	19	91	27	202	72	90
51	−63.8	0.2	−8.77	0.07	n.m.	n.m.	n.m.	n.m.	n.m.	n.m.	n.m.
52	−60.9	0.2	−8.37	0.05	1.9	17	112	18	290	41	66
53	−60.3	0.2	−8.32	0.01	1.2	24	103	28	259	65	100
54	−47.4	0.1	−5.96	0.07	1.2	27	88	24	247	39	115
55	−58.0	0.1	−7.65	0.06	n.m.	n.m.	n.m.	n.m.	n.m.	n.m.	n.m.
56	−59.1	0.1	−7.95	0.03	n.m.	n.m.	n.m.	n.m.	n.m.	n.m.	n.m.
57	−65.4	0.1	−9.02	0.05	1.8	22	95	34	293	21	108

[a]Values for isotope values are ‰, Vienna standard mean ocean water; values for chemical data are mg/L. Abbreviation is as follows: n.m., not measured.

patterns of age with distance can often be explained by corresponding patterns in the depth-distance distribution of the well screens. In contrast, the piedmont samples show a rather clear and linear increase of age with sample depth (Figure 4b).

[29] Stable isotope (δ^{18}O) values are listed in Table 3 and shown versus distance and depth in Figure 5. Here and in the following discussion we focus on δ^{18}O for simplicity, but δ^2H shows very similar patterns and could be used equally well. Clear trends of decreasing δ^{18}O values with distance and depth are visible. The shallow mountain well 54 with its exceptionally enriched isotopic signature appears as an outlier in Figure 5. A decreasing trend of δ^{18}O with depth in the NCP was already noted by *Lu et al.* [2008]. The horizontal δ^{18}O trend also extends downstream of the present study area, where it can be interpreted in terms of paleoclimatic variations [*Kreuzer et al.*, 2009]. However, climatic influences are not expected to be significant in the group of relatively young samples discussed here, which all are of modern and submodern age. Note that the horizontal trend cannot be explained by the continental effect, which would imply a decrease of stable isotope ratios with distance from the coast, whereas our distance scale is directed from the mountains to the coast. The enriched isotopic signature of the mountain samples is also in contradiction to the altitude effect. A possible influence of the amount effect is difficult to assess, as we do not have spatially resolved data on precipitation amounts. However, a large variation of precipitation over the relatively small main recharge area in the piedmont is unlikely.

[30] Major ion concentrations (Table 3) are available for most of the wells. They generally show only moderate variability within the study area and no significant trends with distance or depth. The same is true for groundwater temperature and electrical conductivity (Table 1). In addition, the noble gas–derived quantities, excess air (expressed by the relative Ne excess, ΔNe), and radiogenic He (Table 2) do not show clear trends with distance or depth. Radiogenic He has been discussed by *Kreuzer et al.* [2009]. While there is a systematic increase with distance and age in the old groundwater of the deep confined aquifers, the distribution of radiogenic He among the young samples studied here is dominated by some unexpectedly high values in the mountain samples and along the southern flowline that passes through the piezometric depression cone of Shijiazhuang. These high radiogenic He values may be due to the proximity of the bedrock near the limit of the NCP and to pumping-induced mixing within the depression cone.

5. Discussion: Groundwater Age and Recharge

[31] The origin of groundwater recharge is an important question for the groundwater management in the NCP. A fundamental question concerns the relative importance of lateral inflow from the Taihang Mountains and areal recharge within the piedmont region. *Chen et al.* [2003b] found a decrease of tritium concentrations both with depth and with horizontal distance over large areas of the NCP, from which a vertical flow velocity of 2.5 m/yr and a horizontal velocity of 1.5 km/yr were estimated. Lateral inflow from the Taihang Mountains was postulated to be the main recharge component. Tracing the nitrate contamination from wastewater irrigation in a smaller area southeast of Shijiazhuang, *Chen et al.* [2006] confirmed a vertical velocity of 2–2.5 m/yr but found a much smaller horizontal velocity of 42–62 m/yr. These results suggest that areally distributed vertical infiltration, either of precipitation and surface water [*Fei*, 1988] or of irrigation return flow [*Kendy et al.*, 2004], rather than lateral inflow, is the dominant recharge mechanism.

[32] Our tritium data (Figure 2) show a more abrupt transition than those of *Chen et al.* [2003b]. Within the unconfined region, no systematic change with distance or depth is apparent. Although the tritium data do not provide detailed age information, they clearly show that water younger than about 50 years is present throughout the unconfined aquifers (even outside the piedmont; see well 44) down to a depth of 80–100 m. While large-scale and fast horizontal flow can neither be proven nor excluded based on these data, an overall vertical velocity of about 2 m/yr can be inferred. Whereas the tritium data only provide one approximate point in the age-depth relation, the ^{3}H-^{3}He data depicting complete horizontal and vertical age profiles should provide more detailed information on the age distribution within the unconfined region.

[33] Figure 4 shows increasing trends of age with distance and depth for the regular samples in the unconfined region. However, because well depths and distance correlate in this area (Figure 1b), the question arises of which of these trends is more significant. The relationship of age with distance (Figure 4a) appears less clear-cut than that between age and depth (Figure 4b). Irregularities in the former can largely be explained by deviations from the general trend of increasing depth with distance. It appears that the age distribution is more closely linked to depth than to distance.

[34] The distinct trend of increasing age with depth among the "regular" samples comprising the entire piedmont plain along a distance of ~50 km can be considered as representative for the area and indicative of areally distributed recharge. A dominant horizontal flow would be difficult to reconcile with the tracer data, as it would require rather high horizontal flow velocities in the range of kilometers per year. Such high velocities seem unlikely and are in contrast to the findings of *Chen et al.* [2006]. The increasing aquifer thickness along the flowline lends further support to these arguments. Given the increasing aquifer volume, the overall groundwater balance must be closed either by a continuous reduction of the horizontal flow velocity toward the east or, more likely, by vertical input. Therefore we conclude that spatially distributed recharge and vertical flow are the dominant processes shaping the age distribution in the unconfined region.

[35] *Solomon et al.* [1993] demonstrated how recharge can be determined from vertical profiles of ^{3}H-^{3}He age at a site with dominantly vertical flow. In this approach, the mean vertical velocity v_z is derived from the slope of a linear fit of the age versus depth, and the recharge rate $r = nv_z$ is finally obtained by multiplication with the effective porosity n. Despite the fact that we do not have vertical age profiles from single sites but only an overall profile for the entire recharge area, it may be possible to use this approach to estimate an effective mean recharge rate for the piedmont plain. Indeed, a linear regression through the regular samples in Figure 4b forced through the origin yields a quite well-defined vertical velocity of (2.6 ± 0.2) m/yr (R^2 = 0.96). However, in order to correctly interpret this result an important complicating factor needs to be taken into account: the spatial and particularly the temporal variability of the water table depth in the study area.

[36] It has to be considered that unlike ^{3}H, the ^{3}H-^{3}He ages do not reflect the entire passage of the water from the land surface to the well screen. Due to the volatility of ^{3}He, the ^{3}H-^{3}He method only dates the residence time of the recharging groundwater after separation from the soil air, that is, under closed conditions in the saturated zone. Therefore, the ^{3}H-^{3}He age is expected to vanish at the water table, not at the land surface [*Solomon et al.*, 1993]. Forcing the fit in Figure 4b through zero would only be justified if the water table had always been close to the surface, which is not the case. Indeed, a free linear regression in Figure 4b yields a smaller slope of 2.0 m/yr and an intercept of 16 m, which may be seen as rough estimate of the mean water table depth in the study area over the last decades. Since the well or screen depth is not a correct measure for the vertical distance to which the apparent ^{3}H-^{3}He ages refer, we calculated the depth of the saturated zone (i.e., screen depth minus depth to water table) for each well.

[37] Figure 6 shows the profile of ^{3}H-^{3}He ages against the calculated saturated depth. An approximately linear tendency of increasing ages with higher saturated depth is apparent for the "regular" samples from the piedmont area (open circles). The fit (straight line in Figure 6), forced through the origin and directly weighted with the depth errors, yields a slope of (1.45 ± 0.13) m/yr (R^2 = 0.90). Forcing the fit through the origin seems justified in this case because the ^{3}H-^{3}He age should vanish at the groundwater table, that is, at zero saturated depth. However, the apparent ages show considerable scatter in the upper ~20 m of the saturated zone. This scatter in the upper part of the profile may reflect the spatial variability of recharge due to the localized nature of pumping and irrigation. The effect of spatial variability will be reduced with increasing depth due to mixing of water originating from a larger surface area. Another conceivable reason for the age scatter near the water table is that the boundary condition of atmospheric He in the soil air is not always perfectly fulfilled at the bottom of the rather deep unsaturated zone [*Hall et al.,* 2005]. Nevertheless, a linear fit with a free intercept yields a similar slope of (1.53 ± 0.30) m/yr (R^2 = 0.64) (dotted line in Figure 6) with an intercept of (−2.1 ± 7.5) m, which includes the origin within the error.

[38] Although Figure 6 yields a rather firm estimate of a vertical velocity of about 1.5 m/yr, the question arises about the precise meaning of this velocity, considering that the saturated depth refers to the present-day water table, which most likely was at a higher level in the past, when the sampled water infiltrated. More generally, it may be asked whether an approach assuming linear vertical age profiles is at all appropriate in a non-steady-state situation of a falling water table as in the NCP case. Indeed, by evaluating linear fits of age versus depth we assume a quasi steady state with a constant vertical velocity over the last 35 years. On one hand, this simplification is enforced by the coarseness of the data, and on the other hand, the assumption is motivated by the fact that widespread pumping and irrigation has been going on in the area since the 1960s [*Kendy et al.*, 2004]. Both the pumping rate and the rate of water table decline have remained approximately constant since about 1980. Before that time, pumping varied significantly. It increased after the mid-1960s to reach a peak of about 1000 mm/yr in 1976 before being reduced to around 500 mm/yr at the beginning of the 1980s [*Kendy et al.*, 2004]. In view of the scatter of the apparent ^{3}H-^{3}He ages, the effect of these changes can hardly be resolved in our data. More detailed local age profiles would be needed to resolve the structure of the age increase with depth in response to past changes of the groundwater pumping and recharge regime.

[39] The approximately linear trends of the apparent ages with both absolute screen depth (Figure 4b) and saturated depth (Figure 6) comply with more or less constant recharge conditions within the dating range, thus justifying the assumption of a quasi steady state. In particular, it is important to note that not only may the vertical flow velocity have been approximately constant, but also the water table declined at a roughly uniform rate. The rate of water table drawdown over the last ~30 years in the study area is about 1 m/yr [*Chen et al.*, 2003b; *Kendy et al.*, 2004; *Foster et al.*, 2004; *Yang et al.*, 2002]. As a result, the difference of the absolute vertical flow velocity of a water parcel and the vertical decline rate of the water table should also have been constant. It is this difference, that is, the vertical velocity with respect to the falling water table, that actually measures the amount of new water that has entered the aquifer system over the last decades.

[40] The conception of a superposition of two vertical movements at constant speed explains the difference of the vertical velocities derived from Figures 4b and 6 and clarifies their physical interpretation. The vertical velocity derived from Figure 4b is based on an absolute depth scale and provides a measure of the absolute velocity of the downward moving water parcels. At least for the oldest samples, which infiltrated at a time when the water table was

close to the land surface, the fit passing through the origin yields a reasonable estimate of this vertical velocity of 2.6 m/yr. On the other hand, the vertical velocity derived from Figure 6 refers to a relative depth scale, namely the distance traveled in the saturated zone with respect to the present-day water table. The fact that the water table has moved downward by approximately 1 m/yr is intrinsically taken into account by this relative scale. Therefore the linear fits in Figure 6 yield a correspondingly lower relative vertical velocity of about 1.5 m/yr.

[41] The above interpretation becomes particularly clear if the differences of the two depth scales for the oldest and deepest samples (wells 40, 48, and 49) are considered. These samples represent water that infiltrated more than 30 years ago at a time when groundwater tables were little affected by pumping. The absolute screen depth used in Figure 4b is therefore an approximately correct estimate of the vertical distance by which these water parcels moved downward in the saturated zone. In a time span of 30–35 years they reached depths of 80–90 m, consistent with the vertical velocity of 2.6 m/yr obtained from Figure 4b. In the meantime, however, the water table also moved downward by about 30 m (1 m/yr), therefore these water parcels are now only some 50 to 60 m below the water table (Figure 6). Obviously, using this latter depth below the water table yields vertical velocities that are about 1 m/yr lower, consistent with the value of 1.5 m/yr derived from Figure 6.

[42] The value of 1.5 m/yr reflects the relative vertical velocity by which the water parcels move ahead of the falling water table and hence the rate of annual input of new groundwater. If this input is ascribed to areally distributed vertical infiltration, it can be translated into an effective recharge rate. Assuming an effective porosity of 0.2 [*Kendy et al.*, 2004], we obtain a recharge rate of 0.3 m/yr.

[43] Because this estimate is obtained from a general vertical age trend observed over a large area, it certainly does not reflect actual vertical infiltration at individual locations, which may be very variable. *Kendy et al.* [2004] modeled recharge rates ranging from 0.05 to 1.09 m/yr, depending on the quantity of irrigation applied. The value of 0.3 m/yr may rather be seen as an effective recharge rate for the entire area, which includes all contributions affecting the age distribution: areally distributed infiltration, recharge from surface water, and possible lateral contributions within the regional eastward groundwater flow from the Taihang Mountains. As natural surface water flow is mostly inexistent, it can only contribute in exceptional flood years. As discussed above, strong lateral inflow is not supported by the age distribution (Figure 4). Furthermore, this component may not contribute much to the net water balance at specific locations because lateral inflows and outflows may be balanced [*Kendy et al.*, 2004]. Therefore, our rather crude estimate may nevertheless be a realistic approximation of the areal recharge rate.

[44] An effective recharge rate of 0.3 m/yr is quite high compared to the mean precipitation of little more than 0.5 m/yr. Because usually only a minor fraction of the precipitation contributes to the recharge, this result suggests that a substantial part of the recharge is made up by irrigation water derived from groundwater pumping. Indeed, our result is consistent with the water balance proposed by *Kendy et al.* [2004]. Precipitation of about 0.5 m/yr and irrigation equivalent to about 0.5 m/yr add up to a total annual water input to the fields of 1 m. About 0.7 m/yr is lost by evapotranspiration, needed to sustain two crops per year, and the remaining 0.3 m/yr is recharged to the unconfined aquifer. The deficit between pumping for irrigation and recharge of about 0.2 m/yr, divided by the specific yield of 0.2, explains the mean observed groundwater table descent of ~1 m/yr. Despite a substantial active recharge of about 0.3 m/yr, the system is in net discharge because the pumping rate exceeds the recharge rate. However, as pointed out by *Kendy et al.* [2004], reduced pumping and irrigation also leads to reduced effective recharge and thus does not stop the water table decline. The true origin of the water balance deficit in the NCP is the difference between evapotranspiration and precipitation.

[45] In summary, our results suggest that irrigation contributes substantially to the recharge in the NCP. Given the strong increase of irrigation and the decline of groundwater tables over the last decades, it is clear that the recharge regime of the unconfined aquifer has experienced substantial anthropogenic alteration. In the following we show that certain aspects of the isotope and tracer data from this area appear to reflect the anthropogenic impact.

6. Anthropogenic Imprint in Tracer Data

[46] Our study area lies in the northern part of the area affected by the East Asian monsoon. Therefore, the variability in the stable isotope composition of precipitation is determined by both temperature and the amount of precipitation [*Johnson and Ingram*, 2004]. During the past 35,000 years, $\delta^{18}O$ values in groundwater showed a systematic decrease with age [*Kreuzer et al.*, 2009]: about −8‰ in the youngest modern samples, −9‰ in the submodern and late Holocene samples, −10‰ in the early Holocene, and −10.5‰ to −11‰ in the late Pleistocene. The variability of $\delta^{18}O$ within the individual sections of this record, representing different climatic conditions, does not exceed 0.5‰ except for the youngest, modern age group. This group, which corresponds to the ^{3}H-^{3}He-dated samples discussed here, shows a comparatively large variation of ~1.4‰. The modern samples also show a substantial variability in noble gas temperatures [*Kreuzer et al.*, 2009], as well as in excess air (ΔNe). The question arises whether this enhanced variability may be related to the anthropogenic alterations of the recharge regime.

[47] The $\delta^{18}O$ values of the modern samples show a decreasing trend not only with distance and depth (Figure 5), but also with ^{3}H-^{3}He age (Figure 7); that is, $\delta^{18}O$ increased over the last 40 years. Since geographic (continental, altitude) effects cannot explain the shift of the stable isotopes, presumably a temporal change of the isotopic signature of the recharging groundwater is at the origin of the observed trends. As observed for other parameters before, the temporal trend of $\delta^{18}O$ is clearly expressed only in the "regular" samples from the piedmont. The mountain samples show the highest stable isotope ratios (one of them extremely high), which may be due to recharge of surface water influenced by evaporation in these local flow systems. The samples from the depression cone presumably are simply shifted toward anomalously young ages.

[48] The change of stable isotope values observed in the modern groundwater is similar in magnitude to differences observed over much longer periods of the entire paleoclimate record from the NCP. As reported by *Kreuzer et al.*

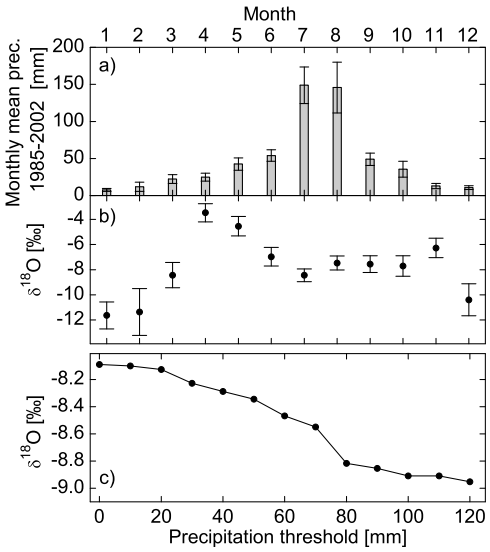

Figure 8. Statistical analysis of the incomplete data set of monthly mean stable isotopes in precipitation of the station Shijiazhuang between 1985 and 2002 [*International Atomic Energy Agency*, 2004]. (a) Mean monthly precipitation (error bars = error of the mean), (b) precipitation-weighted mean monthly $\delta^{18}O$ value (error bars = error of the mean), (c) overall precipitation-weighted mean $\delta^{18}O$ value for the data period, including only months with precipitation above a certain threshold.

[2009], the record contains two periods with trends toward heavier $\delta^{18}O$ compositions by about 1‰, one between the Pleistocene and the Holocene, and one within the Holocene. Based on the comparison with noble gas recharge temperatures, the former can be ascribed to a temperature effect, whereas the latter is not related to temperature but rather to a decrease in monsoon intensity. In the short ~40 year period covered by the modern samples, neither an increase of temperature nor changes in precipitation are likely to be responsible for the observed enrichment in ^{18}O. At best, a small part of the trend might be ascribed to the recent warming in the area. The temperature data from Shijiazhuang (http://www.bcc.cma.gov.cn) show a warming trend of 0.3°C per decade between 1955 and 1999. As the temperature sensitivity of $\delta^{18}O$ derived from recent precipitation at regional stations ranges from 0.11‰/°C to 0.15‰/°C [*Kreuzer et al.*, 2009], the modern warming explains at most an increase of $\delta^{18}O$ of about 0.2‰.

[49] It appears more likely that the recent enrichment trend is the result of the anthropogenic impact on the upper NCP groundwater layers, in particular the changing recharge sources and rates. In this respect, it is interesting to note that the stable isotope signature of groundwater in the NCP differs considerably from the isotopic composition of the mean precipitation. Direct precipitation-weighted averaging of the incomplete set of monthly stable isotope data of Shijiazhuang from 1985 to 2002 [*International Atomic Energy Agency*, 2004] yields a mean value of −8.1‰ for $\delta^{18}O$ (−56.7‰ for $\delta^{2}H$). However, this value appears to be biased by the uneven representation of different months in the data set, coupled with systematic seasonal changes of precipitation amount and isotopic composition. Figures 8a and 8b show separately averaged values of precipitation amount and $\delta^{18}O$ for each month over the years with available data from Shijiazhuang, respectively. Calculating a precipitation-weighted annual mean from these mean monthly data, we obtain −7.5‰ for $\delta^{18}O$ (−52.5‰ for $\delta^{2}H$).

[50] The so calculated mean $\delta^{18}O$ value of modern precipitation is higher than the $\delta^{18}O$ of modern groundwater (−8.2‰ ± 0.4‰) and especially the submodern and late Holocene samples (about −9‰). Assuming that $\delta^{18}O$ of precipitation did not change much over the period covered by these samples, the extent of the isotopic depletion of groundwater compared to precipitation must have changed, and it was particularly strong for the submodern and older samples, which infiltrated under more natural conditions. This depletion can be explained by preferential recharge in the rainy monsoon season, when $\delta^{18}O$ values of precipitation are relatively low (Figure 8). To illustrate this effect, we calculated the mean isotopic composition of the recharging groundwater under the simplified assumption that only months with a certain minimum of precipitation contribute to the recharge [*Kreuzer*, 2007]. Figure 8c shows the mean $\delta^{18}O$ values of precipitation of the months exceeding a certain precipitation threshold as a function of the threshold value. These values were calculated as the mean of the available monthly $\delta^{18}O$ values over the years 1985–2002 weighted with precipitation amount, not from the beforehand calculated monthly means shown in Figures 8a and 8b. Figure 8c illustrates that the isotopic composition of the recharging groundwater may approach the lower values of submodern and late Holocene groundwater (~−9‰) if only periods with substantial monthly precipitation contribute.

[51] If preferential recharge in the monsoon season is a valid explanation of the comparatively low $\delta^{18}O$ values of the samples older than about 30 years, a weakening of this preference (i.e., a lowering of the precipitation threshold) could potentially explain the increase of the $\delta^{18}O$ values in the younger groundwater. The modern irrigation regime leads to wet soils and recharge of irrigation water also during the dry season. This soil preconditioning may favor year-round infiltration of precipitation and therefore shift the isotopic composition of the groundwater toward the mean of precipitation. However, this effect should be counteracted by the contribution of the applied irrigation water to the recharge, which typically is older groundwater with more negative $\delta^{18}O$ values than precipitation. Therefore, a possible change of the seasonality of recharge can hardly explain the full change of observed stable isotope values.

[52] The classical stable isotope plot of $\delta^{2}H$ versus $\delta^{18}O$ (Figure 9) may help to identify mixing and other processes affecting the isotopic composition of the groundwater. The trend defined by the modern samples in this figure does not include the point representing the weighted mean of the precipitation (cross), thus ruling out simple mixing between a depleted submodern groundwater component and modern yearly mean precipitation. Instead, the modern samples follow a well-defined regression line ($R^2 = 0.97$) with a slope of 6.1 ± 0.3, significantly lower than the global meteoric water line slope of 8 and the similar slope applying for the older groundwater of the entire rest (covering the last ~35,000 years) of the data set of *Kreuzer et al.* [2009]. Of interest, this trend for the modern groundwater includes both the "regular" samples from the piedmont plain and the highly enriched samples from the mountain area. If the samples from the mountain valleys and the Shijiazhuang depression

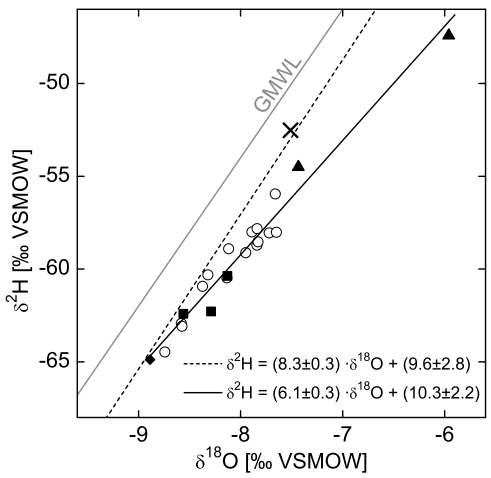

Figure 9. Stable isotope plot showing δ^2H versus δ^{18}O. Symbols as in Figure 2. The solid black line is a fit to modern samples with ^{3}H-^{3}He ages <36 years; the dashed black line is a fit to older samples outside of the ^{3}H-^{3}He dating range from a more extensive NCP data set [*Kreuzer at al.*, 2009]; the solid gray line is the global meteoric water line (GMWL). The cross denotes a mean value for precipitation obtained from the available Global Network of Isotopes in Precipitation data of Shijiazhuang (1985–2002) by averaging the mean monthly values of Figure 8b weighted with the mean monthly precipitation amounts of Figure 8a.

cone are excluded from the regression in Figure 9, the slope and even its uncertainty change only little to 6.3 ± 0.4 (R^2 = 0.93).

[53] A slope lower than 8 can generally be interpreted as an indication of evaporation. In our case, the fact that the most-enriched mountain samples lie on the regression line defined by the piedmont samples may also indicate admixing of mountain-type water to the recharging groundwater in the plain. Even in this case, however, the ultimate cause of the enrichment may be evaporation, for example, from rivers and reservoirs in the mountain area. This enriched water may reach the recharge area in the piedmont by lateral inflow in the subsurface or via surface water flow followed by its use for irrigation. Some of the most enriched samples from the piedmont are found relatively close to the edge of the plain or to surface water features (e.g., well 1 next to the Huangbizhuang reservoir; see Figure 1).

[54] In general the dominant source of irrigation water, which contributes to the recharge by reinfiltration, is groundwater. If the pumped groundwater is older than a few decades, it should have a somewhat depleted isotopic signature compared to modern precipitation and groundwater. The δ^{18}O values of the reinfiltrating part of the irrigation water, however, may be affected by evaporation during the extensive flooding of the fields. The signal of increasing δ^{18}O over time might then be caused by the continuous recycling of groundwater used for irrigation. The youngest and shallowest water may already have experienced multiple pumping-irrigation-reinfiltration cycles, where each cycle slightly enriched the isotopic signature due to evaporation. Even in the case of municipal rather than agricultural water use, evaporation may play a role. For example, *Chen et al.* [2006] identified evaporation to explain the enriched isotopic signature of wastewater in the Shijiazhuang area.

[55] Another indicator for recharge conditions is provided by the size of the excess air component dissolved in groundwater, typically expressed as the relative Ne excess, ΔNe. This parameter mainly reflects the amplitude of groundwater table fluctuations, as higher water table increases promote the dissolution of entrapped air bubbles [*Aeschbach-Hertig et al.*, 2002; *Beyerle et al.*, 2003; *Holocher et al.*, 2003]. In the NCP, ΔNe is relatively low and quite uniform around 20% over the past 35,000 years [*Kreuzer*, 2007; *Kreuzer et al.*, 2009]. Of interest, values of ΔNe below 10% occur almost exclusively in the submodern age group, and values above 25% occur predominantly in the modern group. Among the modern samples from the piedmont plain, ΔNe varies between about 10% and 60% (Table 2). The exceptionally high ΔNe values in some of the modern wells suggest that unusually large water table fluctuations have occurred in the recent decades. It is conceivable that the pumping during the dry part of the year has increased the seasonal water table fluctuations. For example, *Kendy et al.* [2004] show historical water level data from the Luancheng Agro-Ecological Research Station near Shijiazhuang, where seasonal water table rises of 2–3 m are not uncommon. Such fluctuations could produce ΔNe values between 40% and 60% [*Aeschbach-Hertig et al.*, 2002; *Ingram et al.*, 2007; *Klump et al.*, 2008].

[56] Despite the systematic distribution of ΔNe between the age groups, clear trends of ΔNe with distance, depth, and age among the young samples are hardly discernible. Only within the central part of the piedmont region along the main sampled cross section does a trend of increasing ΔNe with increasing δ^{18}O values appear to exist. This trend might indicate that the samples most affected by the recent increase of δ^{18}O are from regions that have experienced more pronounced water table fluctuations, which may be related to groundwater pumping. This finding may be seen as additional evidence that the variation of δ^{18}O in the modern groundwater is related to recharge conditions also in response to groundwater use for irrigation rather than to changes in precipitation and climate.

7. Conclusions

[57] The ^{3}H-^{3}He method provides reliable estimates of the groundwater residence time in the unconfined aquifers of the NCP and therefore is well suited to study groundwater recharge in the piedmont region. All wells within the supposed recharge area, the unconfined part of the piedmont plain, contain substantial tritium concentrations and can easily be dated. Corrections for excess air and radiogenic He are moderate and can confidently be applied based on good fits of the CE model to atmospheric noble gases and He isotope data from much older, tritium-free samples farther downstream [*Kreuzer et al.*, 2009]. Although most of our sampled wells follow a hypothetical flowline along a transect from the Taihang Mountains into the central plain, a clear age evolution along this line is not apparent within the unconfined region of the piedmont plain. In contrast, ^{3}H-^{3}He ages correlate with screen depth in this region, indicating that areally distributed infiltration is the main recharge mechanism.

[58] Relating the ^{3}H-^{3}He ages to the depth of the saturated zone at each well takes into account that the groundwater table has continuously fallen in the area over the period

of about 35 years represented by the groundwater ages. From the correlation of age with saturated depth we derive an effective recharge rate of ~0.3 m/yr, which apparently has been relatively constant during this time. Given that precipitation is not much higher (~0.5 m/yr) and surface water is virtually inexistent, return flow of groundwater used for irrigation must contribute substantially to this recharge rate. This result is in good agreement with model-based estimates of *Kendy et al.* [2004] and confirms their conclusion that a deficit of about 0.2 m/yr, corresponding to the difference between evapotranspiration and precipitation, exists in the NCP. This deficit is currently compensated for by groundwater mining and translates into a water table decline of about 1 m/yr. As reduced pumping and irrigation also reduces effective recharge, this deficit can only be sustainably balanced by reducing evapotranspiration (i.e., changes in crop growing) or by importing surface water into the NCP.

[59] Obviously, anthropogenic changes of the water balance have substantially altered the recharge regime of the unconfined aquifer. An intriguing finding of our study is that this modification appears to be imprinted in the stable isotope signature of the modern groundwater. The systematically increasing enrichment of $\delta^{18}O$ over the last few decades is as large as natural climate-related changes that occurred over the last 20,000 years. Several factors may contribute to the recent increase of $\delta^{18}O$ values in the groundwater, such as less seasonality in the fraction of precipitation that contributes to recharge, a higher contribution of enriched water from the adjacent mountain area, or evaporation during flood irrigation in the pumping and reinfiltration cycles. Unusually high ΔNe values in some of the modern samples from the recharge area may be related to increased seasonal water table fluctuations due to pumping. Certainly further studies are needed to clarify to what extent tracers such as $\delta^{18}O$ and ΔNe can be used to improve our understanding of the recharge conditions and mechanisms in the NCP.

[60] **Acknowledgments.** We thank numerous members of the Institute of Hydrogeology and Environmental Geology, Zhengding, for support of the field work, Michael Sabasch for stable isotope, and Martin Wieser for tritium analyses. Constructive comments by A. Herczeg, A. Suckow, and an anonymous reviewer were very helpful in improving the manuscript. This work was financially supported by the German Science Foundation (DFG grant AE 93/1) and by the National Natural Science Foundation of China (NSFC grant 40472125).

References

Aeschbach-Hertig, W., P. Schlosser, M. Stute, H. J. Simpson, A. Ludin, and J. F. Clark (1998), A $^3H/^3He$ study of groundwater flow in a fractured bedrock aquifer, *Ground Water*, *36*, 661–670, doi:10.1111/j.1745-6584.1998.tb02841.x.

Aeschbach-Hertig, W., F. Peeters, U. Beyerle, and R. Kipfer (1999), Interpretation of dissolved atmospheric noble gases in natural waters, *Water Resour. Res.*, *35*, 2779–2792, doi:10.1029/1999WR900130.

Aeschbach-Hertig, W., F. Peeters, U. Beyerle, and R. Kipfer (2000), Palaeotemperature reconstruction from noble gases in ground water taking into account equilibration with entrapped air, *Nature*, *405*(6790), 1040–1044, doi:10.1038/35016542.

Aeschbach-Hertig, W., U. Beyerle, J. Holocher, F. Peeters, and R. Kipfer (2002), Excess air in groundwater as a potential indicator of past environmental changes, in *Study of Environmental Change Using Isotope Techniques*, pp. 174–183, Int. Atomic Energy Agency, Vienna.

Aeschbach-Hertig, W., H. El-Gamal, M. Wieser, and L. Palcsu (2008), Modeling excess air and degassing in groundwater by equilibrium partitioning with a gas phase, *Water Resour. Res.*, *44*, W08449, doi:10.1029/2007WR006454.

Beyerle, U., J. Rüedi, M. Leuenberger, W. Aeschbach-Hertig, F. Peeters, R. Kipfer, and A. Dodo (2003), Evidence for periods of wetter and cooler climate in the Sahel between 6 and 40 kyr BP derived from groundwater, *Geophys. Res. Lett.*, *30*(4), 1173, doi:10.1029/2002GL016310.

Chen, Z. Y., J. X. Qi, J. M. Xu, J. M. Xu, H. Ye, and Y. J. Nan (2003a), Paleoclimatic interpretation of the past 30 ka from isotopic studies of the deep confined aquifer of the North China plain, *Appl. Geochem.*, *18*, 997–1009, doi:10.1016/S0883-2927(02)00206-8.

Chen, J. Y., C. Y. Tang, Y. J. Shen, Y. Sakura, A. Kondoh, and J. Shimada (2003b), Use of water balance calculation and tritium to examine the dropdown of groundwater table in the piedmont of the North China Plain (NCP), *Environ. Geol.*, *44*, 564–571, doi:10.1007/s00254-003-0792-3.

Chen, J. Y., C. Y. Tang, Y. Sakura, A. Kondoh, J. J. Yu, J. Shimada, and T. Tanaka (2004), Spatial geochemical and isotopic characteristics associated with groundwater flow in the North China Plain, *Hydrol. Process.*, *18*, 3133–3146, doi:10.1002/hyp.5753.

Chen, Z. Y., Z. L. Nie, Z. J. Zhang, J. X. Qi, and Y. J. Nan (2005), Isotopes and sustainability of ground water resources, North China Plain, *Ground Water*, *43*, 485–493, doi:10.1111/j.1745-6584.2005.0038.x.

Chen, J. Y., C. Y. Tang, and J. J. Yu (2006), Use of ^{18}O, ^2H and ^{15}N to identify nitrate contamination of groundwater in a wastewater irrigated field near the city of Shijiazhuang, China, *J. Hydrol. Amsterdam*, *326*, 367–378, doi:10.1016/j.jhydrol.2005.11.007.

Clark, I. D., and P. Fritz (1997), Identifying and dating modern groundwaters, in *Environmental Isotopes in Hydrogeology*, edited by I. D. Clark and P. Fritz, pp. 171–197, Lewis, Boca Raton, Fla.

Cook, P. G., and D. K. Solomon (1997), Recent advances in dating young groundwater: Chlorofluorocarbons, $^3H/^3He$ and ^{85}Kr, *J. Hydrol. Amsterdam*, *191*, 245–265, doi:10.1016/S0022-1694(96)03051-X.

Doney, S. C., D. M. Glover, and W. J. Jenkins (1992), A model function of the global bomb tritium distribution in precipitation, 1960–1986, *J. Geophys. Res.*, *97*(C4), 5481–5492, doi:10.1029/92JC00015.

Fei, J. (1988), Groundwater resources in the North China Plain, *Environ. Geol. Water Sci.*, *12*(1), 63–67, doi:10.1007/BF02574828.

Foster, S., H. Garduno, R. Evans, D. Olson, Y. Tian, W. Zhang, and Z. Han (2004), Quaternary aquifer of the North China Plain: Assessing and achieving groundwater resource sustainability, *Hydrogeol. J.*, *12*, 81–93, doi:10.1007/s10040-003-0300-6.

Hall, C. M., M. C. Castro, K. C. Lohmann, and L. Ma (2005), Noble gases and stable isotopes in a shallow aquifer in southern Michigan: Implications for noble gas paleotemperature reconstructions for cool climates, *Geophys. Res. Lett.*, *32*, L18404, doi:10.1029/2005GL023582.

Holocher, J., F. Peeters, W. Aeschbach-Hertig, W. Kinzelbach, and R. Kipfer (2003), Kinetic model of gas bubble dissolution in groundwater and its implications for the dissolved gas composition, *Environ. Sci. Technol.*, *37*, 1337–1343, doi:10.1021/es025712z.

Ingram, R. G. S., K. M. Hiscock, and P. F. Dennis (2007), Noble gas excess air applied to distinguish groundwater recharge conditions, *Environ. Sci. Technol.*, *41*, 1949–1955, doi:10.1021/es061115r.

International Atomic Energy Agency (2004), Global Network of Isotopes in Precipitation, http://www-naweb.iaea.org/napc/ih/IHS_resources_gnip.html, Int. Atomic Energy Agency, Vienna.

Johnson, K. R., and B. L. Ingram (2004), Spatial and temporal variability in the stable isotope systematics of modern precipitation in China: Implications for paleoclimatic reconstructions, *Earth Planet. Sci. Lett.*, *220*, 365–377, doi:10.1016/S0012-821X(04)00036-6.

Kendy, E., P. Gérard-Marchant, M. T. Walter, Y. Q. Zhang, C. M. Liu, and T. S. Steenhuis (2003), A soil-water-balance approach to quantify groundwater recharge from irrigated cropland in the North China Plain, *Hydrol. Process.*, *17*, 2011–2031, doi:10.1002/hyp.1240.

Kendy, E., Y. Q. Zhang, C. M. Liu, J. X. Wang, and T. S. Steenhuis (2004), Groundwater recharge from irrigated cropland in the North China Plain: Case study of Luancheng County, Hebei Province, 1949–2000, *Hydrol. Process.*, *18*, 2289–2302, doi:10.1002/hyp.5529.

Kipfer, R., W. Aeschbach-Hertig, F. Peeters, and M. Stute (2002), Noble gases in lakes and ground waters, in *Noble Gases in Geochemistry and Cosmochemistry*, vol. 47, edited by D. Porcelli et al., pp. 615–700, Mineral. Soc. of Am. Geochem. Soc., Washington, D. C.

Klump, S., O. A. Cirpka, H. Surbeck, and R. Kipfer (2008), Experimental and numerical studies on excess-air formation in quasi-saturated porous media, *Water Resour. Res.*, *44*, W05402, doi:10.1029/2007WR006280.

Kreuzer, A. (2007), Paläotemperaturstudie mit Edelgasen im Grundwasser der Nordchinesischen Tiefebene, Ph.D. thesis, Univ. of Heidelberg, Germany.

Kreuzer, A. M., C. von Rohden, R. Friedrich, Z. Chen, J. Shi, I. Hajdas, R. Kipfer, and W. Aeschbach-Hertig (2009), A record of temperature and monsoon intensity over the past 40 kyr from groundwater in the North China Plain, *Chem. Geol.*, *259*(3–4), 168–180, doi:10.1016/j.chemgeo.2008.11.001.

Lu, Y. T., C. Y. Tang, J. Y. Chen, X. F. Song, F. D. Li, and Y. Sakura (2008), Spatial characteristics of water quality, stable isotopes and tritium associated with groundwater flow in the Hutuo River alluvial fan plain of the North China Plain, *Hydrogeol. J.*, *16*, 1003–1015, doi:10.1007/s10040-008-0292-3.

Schlosser, P., M. Stute, C. Dörr, C. Sonntag, and K. O. Münnich (1988), Tritium/^{3}He dating of shallow groundwater, *Earth Planet. Sci. Lett.*, *89*, 353–362, doi:10.1016/0012-821X(88)90122-7.

Solomon, D. K., S. L. Schiff, R. J. Poreda, and W. B. Clarke (1993), A validation of the ^{3}H/^{3}He-method for determining groundwater recharge, *Water Resour. Res.*, *29*, 2951–2962, doi:10.1029/93WR00968.

Solomon, D. K., R. J. Poreda, P. G. Cook, and A. Hunt (1995), Site characterization using ^{3}H/^{3}He ground-water ages, Cape Cod, MA, *Ground Water*, *33*, 988–996, doi:10.1111/j.1745-6584.1995.tb00044.x.

Tolstikhin, I. N., and I. L. Kamenskiy (1969), Determination of groundwater ages by the T-^{3}He method, *Geochem. Int.*, *6*, 810–811.

Vogel, J. C. (1967), Investigation of groundwater flow with radiocarbon, in *Isotopes in Hydrology*, pp. 355–369, Int. Atomic Energy Agency, Vienna.

Yang, Y. H., M. Watanabe, Y. Sakura, C. Y. Tang, and S. Hayashi (2002), Groundwater-table and recharge changes in the Piedmont region of Taihang Mountain in Goacheng City and its relation to agricultural water use, *Water S.A.*, *28*, 171–178.

Zhang, Z. G., H. P. Zhang, J. C. Sun, L. J. Yang, Y. L. Cui, L. H. Wu, J. X. Qi, and J. M. Xu (1987), Environmental isotope study related to groundwater age, flow system and saline water origin in Quaternary aquifer of Hebei Plain (in Chinese)., *Hydrogeol. Eng. Geol.*, *96*(49), 1–6.

W. Aeschbach-Hertig, A. Kreuzer, and C. von Rohden (corresponding author), Institute of Environmental Physics, University of Heidelberg, D-69120 Heidelberg, Germany. (christoph.vonrohden@iup.uni-heidelberg.de)

Z. Chen, Institute of Hydrogeology and Environmental Geology, Chinese Academy of Geological Sciences, 050803 Zhengding, Hebei, China.

R. Kipfer, Department of Water Resources and Drinking Water, Swiss Federal Institute of Aquatic Science and Technology, CH-8600 Duebendorf, Switzerland.